Published OnlineFirst November 20, 2015; DOI: 10.1158/1078-0432.CCR-15-1272

Personalized Medicine and Imaging

Clinical Cancer Research

ImmunoPET with Anti-Mesothelin Antibody in Patients with Pancreatic and Ovarian Cancer before Anti-Mesothelin Antibody–Drug Conjugate Treatment

Laetitia E. Lamberts[1], Catharina W. Menke-van der Houven van Oordt[2], Eva J. ter Weele[1,3], Frederike Bensch[1], Michiel M. Smeenk[1], Johannes Voortman[2], Otto S. Hoekstra[4], Simon P. Williams[5], Bernard M. Fine[6], Daniel Maslyar[6], Johan R. de Jong[7], Jourik A. Gietema[1], Carolien P. Schröder[1], Alphons H.H. Bongaerts[8], Marjolijn N. Lub-de Hooge[3,7], Henk M.W. Verheul[2], Sandra M. Sanabria Bohorquez[6], Andor W.J.M. Glaudemans[7], and Elisabeth G.E. de Vries[1]

Abstract

Purpose: Mesothelin (MSLN) is frequently overexpressed in pancreatic and ovarian cancers, making it a potential drug target. We performed an ^{89}Zr-PET imaging study with MMOT0530A, a MSLN antibody, in conjunction with a phase I study with the antibody–drug conjugate DMOT4039A, containing MMOT0530A bound to MMAE. The aim was to study antibody tumor uptake, whole-body distribution, and relation between uptake, response to treatment, and MSLN expression.

Experimental Design: Before DMOT4039A treatment, patients received 37 MBq ^{89}Zr-MMOT0530A followed by PET/CT imaging 2, 4, and 7 days postinjection. Tracer uptake was expressed as standardized uptake value (SUV). MSLN expression was determined with immunohistochemistry (IHC) on archival tumor tissue.

Results: Eleven patients were included, 7 with pancreatic and 4 with ovarian cancer. IHC MSLN expression varied from absent to strong. Suitable tracer antibody dose was 10 mg MMOT0530A and optimal imaging time was 4 and 7 days postinjection. Tumor tracer uptake occurred in 37 lesions with mean SUV_{max} of 13.1 ($\pm$7.5) on PET 4 days postinjection, with 11.5 ($\pm$7.5) in ($N = 17$) pancreatic and 14.5 ($\pm$8.7) in ($N = 20$) ovarian cancer lesions. Within patients, a mean 2.4-fold ($\pm$1.10) difference in uptake between tumor lesions existed. Uptake in blood, liver, kidneys, spleen, and intestine reflected normal antibody distribution. Tracer tumor uptake was correlated to IHC. Best response to DMOT4039A was partial response in one patient.

Conclusions: With ^{89}Zr-MMOT0530A-PET, pancreatic and ovarian cancer lesions as well as antibody biodistribution could be visualized. This technique can potentially guide individualized antibody-based treatment. *Clin Cancer Res; 22(7); 1642–52.* ©*2015 AACR.*

Introduction

Recognition of tumor-specific molecular characteristics involved in all hallmarks of cancer has led to the development of many targeted cancer drugs (1). Despite the success of targeted cancer drugs, regretfully, for several tumor types, such as pancreatic and ovarian cancer, no important "drugable" targets are available. A promising approach is to use tumor-specific membrane proteins (even those with no known role in tumorigenesis) as targets for toxin delivery by several innovative drug types such as immunotoxins and antibody–drug conjugates (ADC; ref. 2). An interesting target molecule in this respect is the membrane-bound surface glycoprotein mesothelin (MSLN; ref. 3). The biologic function of MSLN is still largely unknown. It is expressed minimally by normal mesothelial cells lining pleural, pericardial, and peritoneal surfaces (4). Interestingly, besides in mesotheliomas, MSLN is also highly overexpressed in 80% to 100% of pancreatic and ovarian cancers (5–8) and to a lesser extent in several other human cancers (3, 8–10).

[1]Department of Medical Oncology, University of Groningen, University Medical Center Groningen, Groningen, the Netherlands. [2]Department of Medical Oncology, VU University Medical Center, Amsterdam, the Netherlands. [3]Department of Clinical Pharmacy and Pharmacology, University of Groningen, University Medical Center Groningen, Groningen, the Netherlands. [4]Department of Radiology and Nuclear Medicine, VU University Medical Center, Amsterdam, the Netherlands. [5]Department of Early Clinical Development, Genentech, Inc. South San Francisco, California. [6]Department of Biomedical Imaging, Genentech, Inc. South San Francisco, California. [7]Department of Nuclear Medicine and Molecular Imaging, University of Groningen, University Medical Center Groningen, Groningen, the Netherlands. [8]Department of Radiology, University of Groningen, University Medical Center Groningen, Groningen, the Netherlands.

Note: Supplementary data for this article are available at Clinical Cancer Research Online (http://clincancerres.aacrjournals.org/).

Corresponding Author: Elisabeth G.E. de Vries, Department of Medical Oncology, University Medical Center Groningen, PO Box 30.001, Groningen 9700 RB, the Netherlands. Phone: 0031-50-3612821; Fax: 0031-50-3614862; E-mail: e.g.e.de.vries@umcg.nl

doi: 10.1158/1078-0432.CCR-15-1272

Published OnlineFirst November 20, 2015; DOI: 10.1158/1078-0432.CCR-15-1272

Translational Relevance

Mesothelin (MSLN) has been recognized as an interesting target for immunotoxins and antibody–drug conjugates (ADC). DMOT4039A, composed of anti-MSLN antibody MMOT0530A and cytotoxic agent MMAE, is evaluated in patients with pancreatic and ovarian cancer. In early drug development, information regarding target presence, organ distribution at the whole-body level, as well as binding of the antibody to the target could be extremely helpful to guide and individualize drug dosing. This study shows that immunoPET with the ^{89}Zr-labeled MMOT0530A is able to visualize whole-body distribution and quantify uptake in pancreatic and ovarian tumor lesions. Whole-body organ-level uptake of the tracer was highest in liver. Tumor lesion uptake between patients and within patients varied. These data support further development of more immunoPET tracers consisting of the "naked" antibody of an ADC to determine whole-body target expression and organs at risk for toxicity, to ultimately guide dosing and confirm delivery of the ADC.

MSLN has been recognized as a potential drug target for more than 10 years. Several approaches to target MSLN have been investigated in clinical trials, such as inducing antibody-dependent cellular toxicity and applying adoptive T-cell immunotherapy (11, 12). An immunotoxin was also developed, with antitumor activity shown in phase I/II studies (13–16). Moreover, a preliminary report about MSLN for drug delivery by an ADC with a maytansinoid cytotoxin showed a partial response (PR) in 1 and stable disease (SD) in 2 mesothelioma patients (17).

Currently, ADCs hold a lot of interest in oncology. Adotrastuzumab emtansine (T-DM1), recently registered by FDA and European Medicines Agency, prolongs progression-free survival (PFS) and overall survival with less toxicity in human epidermal growth factor receptor 2 (HER2)-positive metastatic breast cancer patients compared with the combination of lapatinib with capecitabine (18). Moreover, a dozen ADCs for different antigens are in different phases of development. It would be helpful to safely and accurately predict the behavior of the ADCs in early drug development (19, 20).

Noninvasive antibody imaging using single photon emission computed tomography (SPECT) and PET, that is, immunoPET, can serve this goal. In general, PET provides better spatial and temporal resolution than SPECT based on its physical principle of detecting coincident gamma pairs instead of single gamma rays. ImmunoPET can be used to determine target antigen expression at whole-body level and to provide information about antibody biodistribution and organ pharmacokinetics, information that is usually lacking from phase I study designs (21). Zirconium-89 (^{89}Zr) is the preferred radioisotope for PET imaging of internalizing targets such as MSLN, as it residualizes in the target tissue after cellular internalization, causing increasing tumor-to-normal tissue ratios over time (22). Several studies with ^{89}Zr-immunoPET in cancer patients have shown that after administration of 37 MBq (1 mCi) ^{89}Zr-labeled antibody, quantitative assessment of tumor uptake and whole-body biodistribution is feasible (23–28). Labeling a complete ADC with a radioisotope could lead to instability of the molecule (29, 30). Using the "naked" antibody for PET imaging of the target will, however, also provide insight into drug distribution, because the process that drives tracer uptake (i.e., tissue exposure and penetration, and also expression of the target and internalization of the antibody) is similar and therefore PET with the "naked" antibody of an ADC seems rational.

In human MSLN–expressing tumor-bearing mice, ^{89}Zr-labeled anti-MSLN antibody MMOT0530A showed progressive and antigen-specific tumor uptake on microPET at 1, 3, and 6 days after tracer injection (31). Therefore, we performed a clinical PET imaging study with the "naked" ^{89}Zr-labeled MMOT0530A in conjunction with the phase I study of ADC DMOT4039A, composed of humanized IgG1 monoclonal antibody (mAb) MMOT0530A and the potent mitotic agent monomethyl auristatin MMAE. The aim was to determine and quantify tumor antibody uptake, whole-body distribution, and organ pharmacokinetics in patients with unresectable pancreatic or platinum-resistant ovarian cancer. In addition, the relation between tracer uptake and MSLN expression and response to DMOT4039A treatment was explored.

Patients and Methods

Patient population

Patients with histologically confirmed, unresectable, and/or metastatic pancreatic or platinum-resistant ovarian cancer and measurable disease according to RECIST 1.1, who were included in the phase I study with DMOT4039A (ClinicalTrials.gov identifier NCT01469793) in the University Medical Center Groningen (UMCG, Groningen, the Netherlands) or the VU University Medical Center (VUMC, Amsterdam, the Netherlands), were eligible for this imaging study (ClinicalTrials.gov identifier NCT01832116). Other inclusion criteria were Eastern Cooperative Oncology Group (ECOG) performance score 0 or 1, adequate bone marrow (absolute neutrophil count $\geq 1.5 \times 10^9$/L, hemoglobin ≥ 9 g/dL, and platelet count $\geq 100 \times 10^9$/L), liver [total bilirubin $\leq 1.5 \times$ upper limit of normal (ULN) and aspartate aminotransferase and alanine aminotransferase $\leq 2.5 \times$ ULN], and renal function (serum creatinine $\leq 1.5 \times$ ULN). Major exclusion criteria were history of severe allergic reactions to antibody therapies and prior treatment with MSLN-targeted therapy. This trial was approved by the Medical Ethical Committee of the UMCG and the Central Committee on Research Involving Human Subjects, a competent authority in the Netherlands. All patients provided written informed consent.

Study design

Patients received 37 MBq (1 mCi) ^{89}Zr-MMOT0530A (effective radiation dose of approximately 18–22 mSv, based on radiation dosimetry studies of other ^{89}Zr-labeled antibodies with comparable characteristics; refs. 32, 33) intravenously and were observed for 1 hour to detect any infusion-related adverse events. To determine the suitable tracer dose, the first cohort of two patients received ^{89}Zr-labeled MMOT0530A (~1 mg) without any additional unlabeled antibody. In the second cohort, the radiolabeled antibody was complemented with unlabeled antibody to a total amount of 10 mg MMOT0530A. The unlabeled antibody was coinfused with the ^{89}Zr-labeled antibody. To determine the optimal antibody tracer dose, the distribution of the tracer in the body as a whole was analyzed. From other antibody tracers, we know that an additional dose of unlabeled antibody is often needed for imaging. When the amount of tracer still present at day 7 postinjection is high enough to visualize the circulation clearly,

Published OnlineFirst November 20, 2015; DOI: 10.1158/1078-0432.CCR-15-1272

we consider this to be the consequence of an adequate protein dose in the tracer. To determine the optimal day for PET scanning, we analyzed all lesions and all organs at all 3 PET scans for each patient. The PET moment on which an adequate tracer amount was present in the circulation and most tumor lesions in most patients had maximum tracer uptake was considered to be the best PET scan.

Clinical grade ^{89}Zr-MMOT0530A was produced in the UMCG essentially as was described previously (31, 34). PET scans were acquired from the top of the skull to mid-thigh with a 64-slice PET/CT camera (Biograph mCT, Siemens in the UMCG and Gemini TF or Ingenuity TF, Philips in the VUMC), for 5 minutes per bed position at day 2 and 4, and 10 minutes per bed position at day 7 after tracer injection. For attenuation and scatter correction, immediately after the PET scan, a low-dose CT scan was acquired with the same PET/CT camera, as part of the same procedure.

Diagnostic CT scans were performed within 21 days before tracer injection and after every 2 cycles of DMOT4039A. CT scans were evaluated centrally at UMCG for measurable lesions according to RECIST 1.1 (35). After the last PET scan (either on the same day or within a week thereafter), patients continued in the phase I study and received treatment with DMOT4039A (36). Archival tumor tissue (both primary and metastatic tissue, if available) was tested for MSLN expression with an immunohistochemical assay using 19C3 mouse anti-human antibody (37). Immunohistochemical scoring was based on at least 10% of tumor cells staining positive, scoring 3+ for strong, 2+ for moderate, 1+ for weak, and 0 for <10% cells staining.

^{89}Zr-MMOT0530A PET analysis

All PET scans were reconstructed similarly (256 matrix, 3 iterations, 21 subsets, and 8-mm filters) and visually analyzed by an experienced nuclear medicine physician. All regions with high tracer uptake, compared with normal organs, were further analyzed using diagnostic CT and the number and locations of visible tumor lesions on the PET scan were determined. Quantification of radioactivity concentration in tumor lesions and normal organs was performed using A Medical Image Data Examiner (AMIDE) software (version 0.9.3, Stanford University, Stanford, CA; ref. 38). In addition to the amount of injected activity and bodyweight, the amount of radioactivity within a lesion or organ served to determine the standardized uptake values (SUV). To assess the present radioactivity, three-dimensional spherical volumes of interest (VOI) were manually drawn around tumor lesions. To assess the biodistribution of the tracer background, VOIs were drawn in the circulation (measured in the left ventricle), liver, spleen, kidney, intestine, lung, brain, bone marrow, femur head, and thigh muscle. To assess the radioactivity concentration in tumor lesions and organs, SUV_{max} (the maximum voxel intensity in the VOI) was calculated. Tumor-to-blood ratios (TBR) were determined using SUV_{max} in tumor lesions and SUV_{max} in blood pool. In addition, to calculate the percentage of the tracer in the liver, in all PET scans of all patients, the liver was three-dimensionally delineated and the volume of the liver with the corresponding radioactivity concentration present in the liver at that PET moment was calculated. Subsequently, the total liver tracer uptake was expressed as percentage of radioactivity still present in the whole body at that PET scan (hereby correcting for ^{89}Zr-decay and excretion both).

Pharmacokinetic assessments

Blood samples for pharmacokinetic analyses of ^{89}Zr were collected at 5 time points: before and 15 minutes postinjection, as well as at day 2, 4, and 7 postinjection (same days as the PET scans). Radioactivity was measured in 1 mL whole blood samples per time point by use of a calibrated well-type gamma-counter (LKB Instruments). Thereafter, radioactivity (determined in activity per mL) was converted to SUV equivalent values, using weight, injected amount of radioactivity, and moment of blood sampling (thereby correcting for ^{89}Zr decay). The SUV uptake in the circulation determined by PET was correlated to the calculated SUV value in the blood samples at the corresponding days.

In addition, the apparent clearance (Cl), volume of distribution (V_d), and elimination half-life ($t_{1/2}$) of ^{89}Zr-labeled MMOT0530A were calculated using a noncompartmental pharmacokinetic model in the "KINFIT module" of the software package MWPharm v 3.81 (Mediware).

Statistical analyses

Data are presented as mean ± SD. Associations between parameters were calculated using the Pearson correlation test (CP) for two continuous variables and the Spearman correlation test (CS) for one continuous and one categorical variable. An independent *t* test was performed to compare tumor uptake between pancreatic and ovarian cancer lesions. P values < 0.05 were considered significant.

Results

Patient characteristics

Between March 2013 and February 2014, a total of 11 patients (7 patients with pancreatic and 4 patients with ovarian cancer) eligible for participation in the phase I study with DMOT4039A, were consecutively enrolled in this study; 2 men and 9 women with a median age of 62 years (range 44–70) (Table 1). Three primary pancreatic tumors and two primary ovarian tumors were still *in situ* at the moment of trial participation.

^{89}Zr-MMOT0530A PET

The first 2 patients received only ^{89}Zr-labeled MMOT0530A (~1 mg protein dose) without additional unlabeled antibody, the 9 patients thereafter were administered ^{89}Zr-labeled MMOT0530A and unlabeled MMOT0530A antibody in a total amount of 10 mg (range 9.4–10.4). The mean radioactivity at time of injection was 36.78 MBq (±1.26). No infusion-related reactions or adverse events were observed in this imaging study.

Tracer dose and organ distribution. In the first 2 patients, who received approximately 1 mg ^{89}Zr-MMOT0530A, mean SUV_{max} in the circulation (measured in the left ventricle on PET scans) decreased fast from 9.2 (±1.6) on day 2 to 6.0 (±2.0) on day 4 to 3.6 (±0.2) on day 7 postinjection. In the next 9 patients, in whom approximately 10 mg additional cold MMOT0530A was administered, more labeled antibody remained in the circulation with a mean SUV_{max} of 10.2 (±3.2), 8.3 (±2.1), and 6.8 (±2.9) on day 2, 4, and 7 postinjection, respectively (Supplementary Fig. S1A). With a mean SUV_{max} of 6.8 (±2.9) at day 7 postinjection, sufficient tracer was available for ongoing tumor uptake until day 7 postinjection. Moreover, visibility of tracer present in the circulation improved using 10 mg of unlabeled antibody added to the labeled MMOT0530A (Fig. 2A–C). Therefore, a suitable

Published OnlineFirst November 20, 2015; DOI: 10.1158/1078-0432.CCR-15-1272

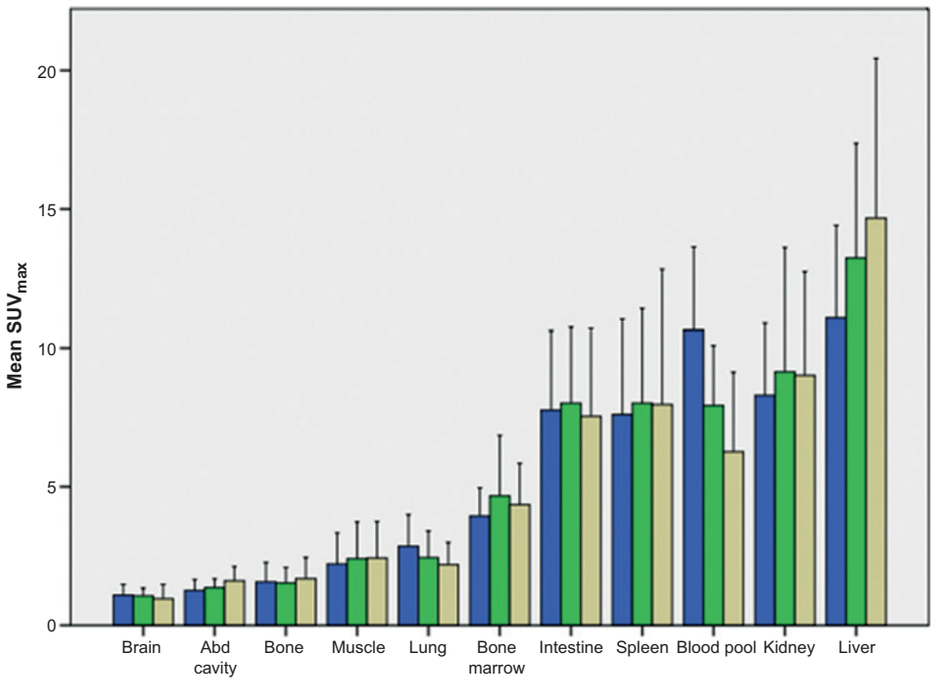

Figure 1.
^{89}Zr-MMOT0530A tracer uptake in normal organs of all patients on PET on 2, 4, and 7 days postinjection in blue, green, and yellow bars ($n = 11$), respectively. Error bars display SD. Abd cavity, abdominal cavity.

tracer dose was determined to be a total of 10 mg MMOT0530A (of which ~1 mg was ^{89}Zr-labeled).

The ^{89}Zr-MMOT0530A organ distribution showed (based on the PET scan 4 days postinjection) a high SUV_{max} in the circulation (7.9 ± 2.2), as well as in the liver (13.2 ± 4.1), kidneys (9.1 ± 4.5), and the spleen (8.0 ± 3.4). The high intestinal mean SUV_{max} at day 4 of 8.0 (± 2.7) reflected excretion with highest uptake in patients with habitual constipation. Low uptake was observed in muscle (2.4 ± 1.3), lung (2.4 ± 1.0), bone (1.5 ± 0.6), and brain tissue (1.1 ± 0.3).

The tracer distribution on the three consecutive PET scans was comparable between patients. The widest ranges were observed for the liver (Supplementary Fig. S1B) and kidneys (Supplementary Fig. S1C) and to a lesser extent also for the blood pool, spleen, and intestine. Mean SUV_{max} in the liver was 11.1 (±3.3), 13.2 (±4.1), and 14.7 (±5.8) and in the kidney 8.3 (±2.6), 9.1 (±4.5), and 9.0 (±3.7) on PET 2, 4, and 7 days post injection, respectively. Mean SUV on PET scan series showed a decline in tracer in the blood pool as expected. The other organs showed stable tracer uptake over time. Figure 1 shows the organ distribution for the PET scans 2, 4, and 7 days postinjection for all patients.

On the PET scans, we determined a mean liver volume of 1.60 L (±0.26 L). The absolute liver uptake was decreasing over time with a radioactivity level of 3.68 MBq (±7.38), 2.58 MBq (±3.57), and 1.39 MBq (±2.76) on PET at days 2, 4, and 7, respectively. However, the percentage injected dose of radioactivity per gram of liver tissue (assuming a tissue density of 1 g/mL; %ID/g) was increasing over time, with a mean %ID/g of 0.82 (±0.30), 1.00 (±0.29), and 1.07 (±0.31) on PET at 2, 4, and 7 days postinjection, respectively. The mean liver uptake at PET 4 days postinjection was in the first cohort 22.5% (22.6% and 22.47%) and in the second cohort 18.2% (±2.4).

The pharmacokinetic variables shown in Table 2 are presented for both cohorts. The ^{89}Zr-MMOT0530A clearance measured in whole blood in cohort 1 was 2-fold faster as compared with cohort 2; with 0.066 L/hour in cohort 1 compared with 0.033 L/hour in cohort 2. Consequently, $t_{1/2}$ was also shorter in cohort 1 (70 hours) than in cohort 2 (105 hours).

Tracer uptake in tumor lesions. ^{89}Zr-MMOT0530A uptake was observed in at least one tumor lesion in all patients (range 1–8 per patient). Representative PET/CT scans from one pancreatic cancer patient are shown in Fig. 2. We used the PET scan of day 4 to present the tumor uptake analyses, as on this PET scan most tumor lesions had maximum uptake and an adequate amount of tracer was available in the circulation (Fig. 3). Because of the decay of ^{89}Zr, the PET scans at day 7 were more difficult to analyze visually and at day 2 tumor uptake did not yet reach its maximum. Mean SUV_{max} of all lesions was 13.1 (±7.5) on PET 4 days postinjection. A total of 37 quantifiable tumor lesions were detected, of which 36 were also visible on the diagnostic CT scan. One lesion, a lymph node in the neck, was positioned outside the field-of-view of the CT scan. Eleven of the 37 lesions were not measurable according to RECIST 1.1 due to being cystic ($n = 3$), peritoneal localization ($n = 4$), or a diameter of <15 mm on the short axis in case of lymph nodes ($n = 4$).

Heterogeneity was present between and within patients as ^{89}Zr-MMOT0530A tumor uptake varied greatly. No clear pattern was found to explain the heterogeneity in tumor uptake. Mean SUV_{max} on PET 4 days postinjection on patient-based analysis was 13.4 (±6.9) with a 5.3-fold difference in mean tumor uptake between patients. The lowest mean SUV_{max} was 5.1 in a patient with pancreatic cancer and the highest was 27.2 in a patient with ovarian cancer. Also, a large intrapatient variation of the tumor SUV_{max} values was found within 8 patients with more than one lesion, with a mean difference of 2.4-fold (±1.1). Mean SUV_{max} on day 4 postinjection was 14.4 (±13.7) for primary tumor lesions ($n = 5$), and 12.9 (±6.4) for metastatic

Published OnlineFirst November 20, 2015; DOI: 10.1158/1078-0432.CCR-15-1272

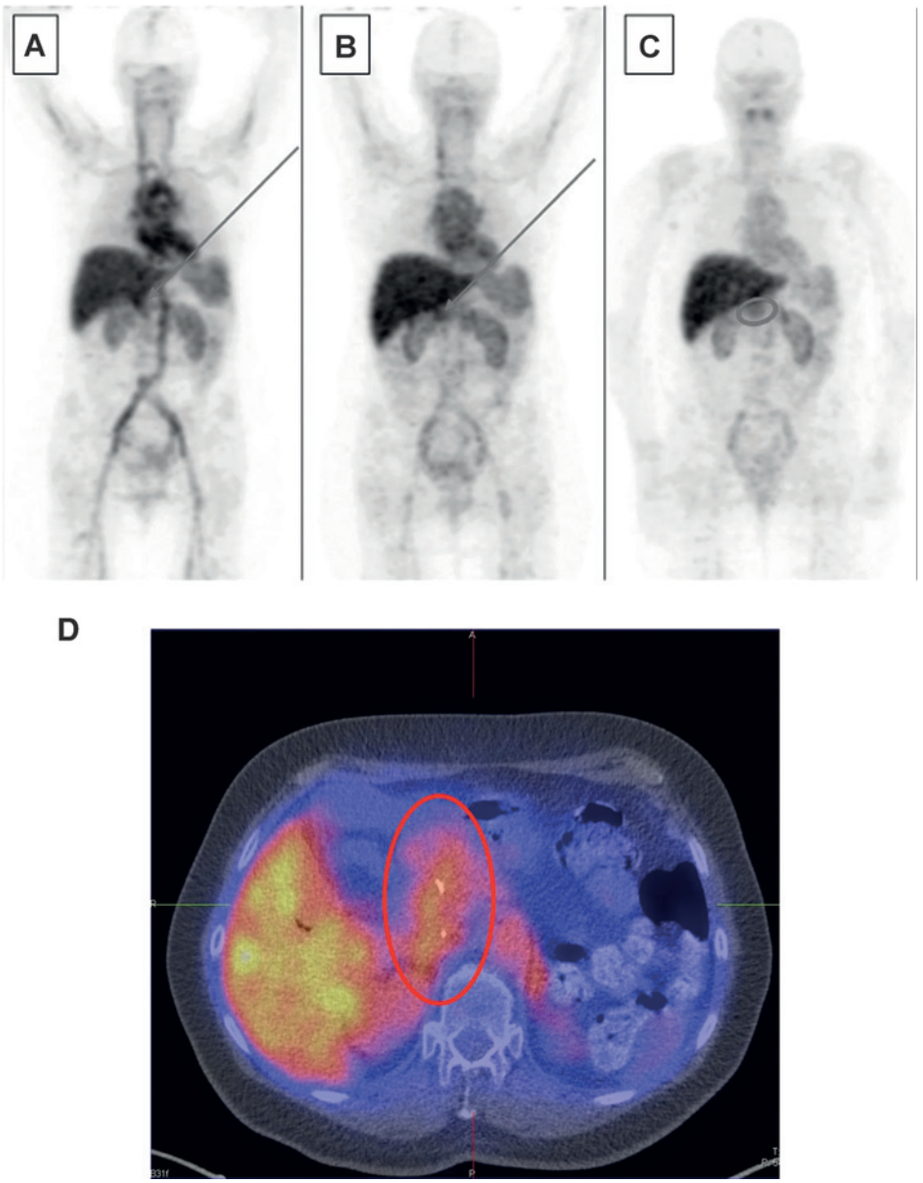

Figure 2.
^{89}Zr-MMOT0530A PET in a pancreatic cancer patient day 2 (A), day 4 (B), and day 7 (C) after tracer injection, showing whole-body distribution with highest uptake in circulation (heart), liver, kidneys, and primary tumor (red circle). A fusion with diagnostic CT shows the primary pancreatic tumor (red circle) and the high liver uptake in healthy liver (D).

lesions. Figure 4 shows tumor uptake for all tumor lesions per patient and per disease.

Tracer uptake differed between lesions of patients with pancreatic and ovarian cancer (Fig. 5). Mean SUV_{max} on day 4 postinjection in lesions of pancreatic cancer ($n = 17$) was 11.5 ($\pm$5.6), while in those of ovarian cancer ($n = 20$) this was 14.5 ($\pm$8.7; $P = 0.221$). Five patients had primary tumors *in situ*. The two primary ovarian cancers had a SUV_{max} of 8.4 and 38.91, respectively. In the primary pancreatic tumors ($n = 3$), mean SUV_{max} was 8.2 ($\pm$0.9). Metastatic tumor lesions of pancreatic origin ($n = 14$) had a mean SUV_{max} of 12.1 ($\pm$6.0), whereas for metastatic lesions of ovarian cancer origin ($n = 18$) this was 13.5 ($\pm$6.9). TBR was rising over time for all except one patient; mean TBR for all patients was 0.9 ($\pm$0.4) at PET 2 days postinjection, 1.7 ($\pm$0.8) and 2.3 ($\pm$1.2) at PET 4 and 7 days postinjection, respectively. In patients with pancreatic cancer, the TBR [0.9 ($\pm$0.4), 1.5 ($\pm$0.8), and 1.9 ($\pm$1.1)] was lower than in patients with ovarian cancer [1.0 ($\pm$0.4), 1.9 ($\pm$0.8), and 2.6 ($\pm$1.3)]. Primary pancreatic lesions had a TBR of 0.70, 1.1, and 1.28 at PET 2, 4, and 7 days postinjection, respectively.

Six measurable lesions on diagnostic CT, according to RECIST 1.1, were not visible on PET. This was the case for one abdominal tumor mass (maximum diameter 30 mm) in a patient with ovarian cancer, for a retroperitoneal lymph node (15 $\times$ 16 mm) in a patient with pancreatic cancer and for 2 lung lesions ($\sim$10 mm) in a patient with pancreatic cancer, and 2 liver lesions (maximum diameters 16 and 11 mm) in a pancreatic cancer patient in whom other liver metastases were visible (uptake did not correspond with metastases on CT). Furthermore, cystic lesions, some peritoneal lesions, and 9 small lymph nodes

Published OnlineFirst November 20, 2015; DOI: 10.1158/1078-0432.CCR-15-1272

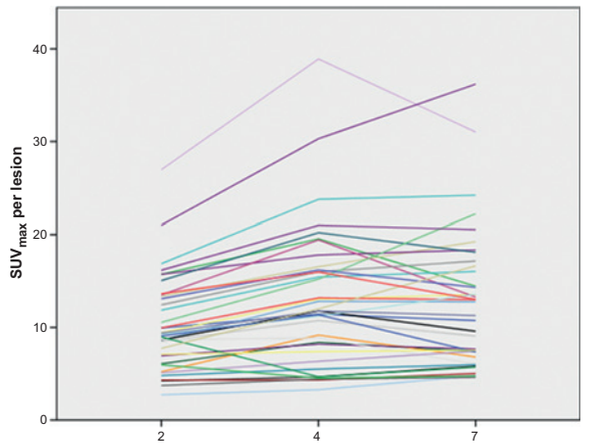

Figure 3.
^{89}Zr-MMOT0530A PET uptake expressed in SUV_{max} (on *y*-axis) on 2, 4, and 7 days, respectively, on *x*-axis for all 37 tumor lesions.

(<15 mm short axis on diagnostic CT) were not visualized on PET. Interestingly, in one patient with pancreatic cancer, high uptake was observed in both adrenal glands (SUV_{max} on day 4 postinjection were 21.6 in the right and 19.9 in the left adrenal gland), while on diagnostic CT, the adrenal glands were classified as fatty adenoma.

Correlation ^{89}Zr-MMOT0530A blood pool activity on PET versus ^{89}Zr activity in blood samples

In 8 patients, whole blood samples for ^{89}Zr activity measurements were available. The SUV equivalents from *ex vivo* measurements of blood samples at 2, 4, and 7 days postinjection correlated well with image-derived SUV values of the blood pool measured by PET (Pearson correlation 0.765, $P = 0.000$; Fig. 6).

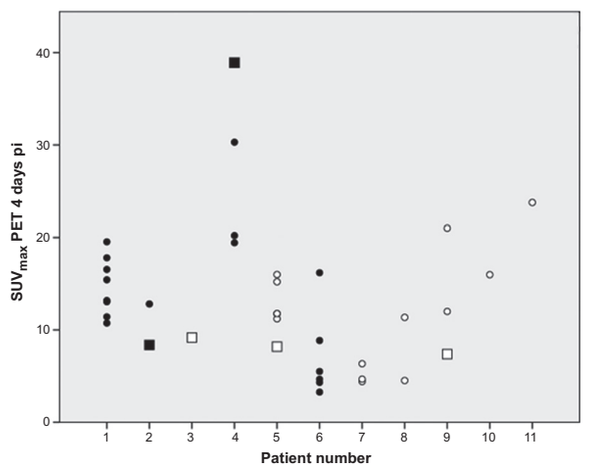

Figure 4.
SUV_{max} values at PET 4 days postinjection of all quantifiable tumor lesions ($n = 37$) plotted per patient on the *x*-axis (7 pancreatic cancer patients with 17 lesions in open dots and 4 ovarian cancer patients with 20 lesions in black filled dots). Squares, primary tumor lesions; circles, metastatic lesions. pi, postinjection.

MSLN IHC expression versus PET uptake

MSLN expression levels determined in primary ($n = 7$) and metastatic ($n = 7$) archival tumor samples varied from 0 to 3+ in 10 patients (Table 1). Primary tissue was available in 3 of the 4 patients with ovarian cancer, and metastatic tumor tissue was available in only 1 patient. Archival tissue was available in 6 of 7 patients with pancreatic cancer, only metastatic tissue in 2 patients, and both primary and metastatic tissue in 4 patients. IHC score was 0 in both primary and metastatic tissue in one patient, while in one patient, the IHC score was higher in primary compared with metastatic tissue (IHC score 3+ vs. 2+). In all others, the immunohistochemical scores were consistent.

On a patient-based analysis, the immunohistochemical score correlated with the mean SUV_{max} per patient on PET day 4 (Spearman correlation 0.689, $P = 0.027$). However, no correlation was found when the two tumor types were analyzed separately. In ovarian cancer, the correlation coefficient was 0.775 ($P = 0.225$). For pancreatic cancer tissue, the correlation coefficient was 0.676 ($P = 0.14$).

Response to DMOT4039A and PET uptake

Five patients received the weekly schedule (dose 0.8–1.2 mg/kg) and 6 patients the every-3-week schedule (dose 2.4–2.8 mg/kg) of DMOT4039A. In 9 of 11 patients, best response was SD, one patient experienced immediate progressive disease (PD), and one patient had a confirmed PR ongoing for 311+ days. Nine patients with stable disease and one with PR had a mean PFS of 121 days (range 28–311+, from start of treatment to PD; ref. 35). PET uptake on a per-patient basis (mean PET uptake over all lesions in one patient) did not correlate with PFS (CP −0.101, $P = 0.768$). On a per-lesion analysis of 26 lesions that were measurable according to RECIST 1.1, there was no correlation between PET uptake and best response on CT in percentage compared with baseline (CP −0.06, $P = 0.786$). The patient with ongoing PR showed PET tracer uptake in 2 liver metastases and in the primary pancreatic tumor (Fig. 7), with SUV_{max} values on PET 4 days postinjection of 21.0, 12.0, and 7.4, respectively.

Discussion

This is the first-in-human study evaluating anti-MSLN antibody tumor uptake and whole-body distribution, using the naked antibody of an ADC with ^{89}Zr-MMOT0530A PET for whole-body antibody distribution. In addition to primary pancreatic and ovarian cancers, metastatic lesions were also visualized.

A relatively small amount of 10 mg MMOT0530A was found to be a suitable protein dose for PET imaging. With a lower protein dose, presence of the tracer in the circulation was too low at day 7 to be optimally visualized and consequently would likely prohibit optimal tumor uptake. The optimal moment for PET scanning was 4 days after tracer injection, because most tumor lesions had maximum uptake at that moment. Although tumor-to-background ratios were lower at day 4 than day 7 they were easier to analyze given the ongoing decay of ^{89}Zr.

Invasive determination of ^{89}Zr in whole blood was completely in line with the PET findings. In patients who received 1 mg antibody (cohort 1), the ^{89}Zr-labeled MMOT0530A half-life was shorter than the patients receiving 10 mg antibody (cohort 2). This is most likely due to faster antibody clearance in the first cohort with the lower antibody dose. For certain antibody-based

Published OnlineFirst November 20, 2015; DOI: 10.1158/1078-0432.CCR-15-1272

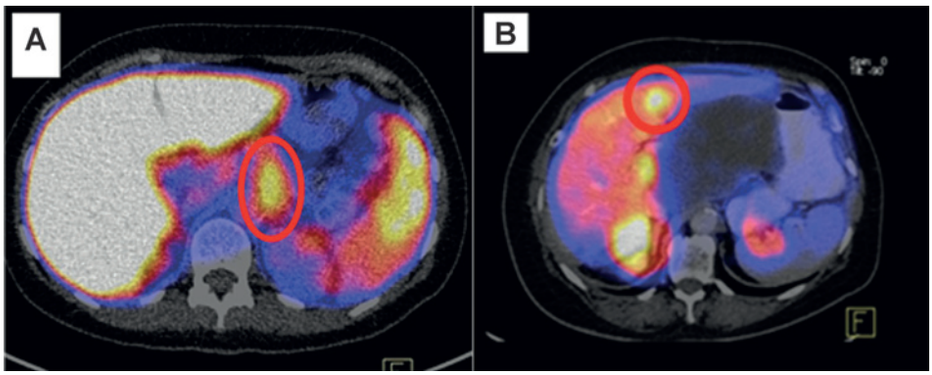

Figure 5.
PET images 4 days postinjection from a patient with pancreatic cancer with the primary tumor (SUV_{max} = 9.17) encircled in red and SUV_{max} of 9.55 in the healthy liver (A); a patient with ovarian cancer with a metastasis in the ligamentum falciparum encircled with SUV_{max} of 16.6. SUV_{max} in the healthy liver is 12.9 (B).

tracers with dose-dependent antibody kinetics, higher doses of unlabeled antibody are needed to counteract the rapid clearance at lower doses (39, 40).

^{89}Zr-MMOT0530A uptake in liver is relatively high and rises over time in contrast to other uptake in other organs. This might be due to hepatic catabolism of MMOT0530A as opposed to target antigen expressed, as MSLN is not normally expressed in normal liver. Hepatic catabolism might be promoted by the antibody complexing with MSLN antigen shed into the circulation. Shedding of antigen into the tumor interstitium is a well-known process for cell-surface proteins including MSLN, which can also influence tumor uptake of MSLN targeting agents in preclinical models (41, 42). However, liver uptake levels of this antibody are comparable with that of other antibodies, such as trastuzumab and huJ591 (26, 43). The high uptake in the liver suggests that it is appropriate to monitor the liver as a potential site of toxicity with the ADC DMOT4039A. In the phase I study, the dose-limiting toxicities were hypophosphatemia and hyperglycemia and clinically significant liver toxicity, expressed as liver function abnormalities, occurred in less than 10% of the patients (36).

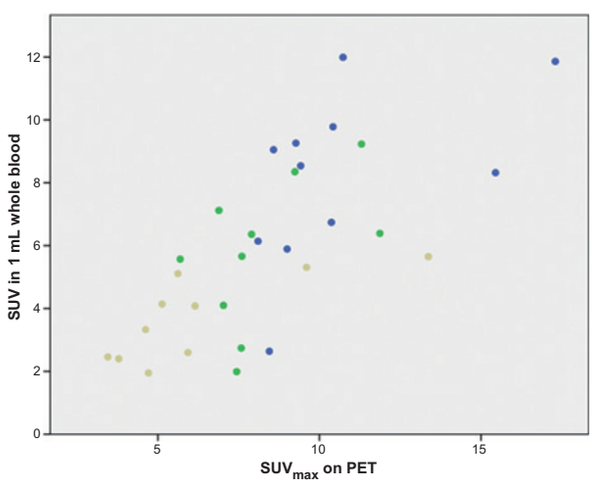

Figure 6.
Correlation between SUV in 1 mL whole blood samples at day 2, 4, and 7 after ^{89}Zr-MMOT0530A injection and SUV_{max} of blood pool as measured in the left ventricle on corresponding PET scans (n = 8 patients). Blue, day 2 postinjection; green, day 4 postinjection; gray, day 7 postinjection. Pearson correlation 0.765, P = 0.000.

^{89}Zr-MMOT0530A tumor uptake was heterogeneous between and within patients. We observed a mean 5.3-fold difference between, and 2.4-fold difference within patients. Inter- and intrapatient heterogeneity is a widely acknowledged phenomenon in oncology, especially since the multiregion sequencing of tumor samples from primary renal carcinomas and their metastatic sites showed in 4 patients that target heterogeneity was not only present between different lesions within one patient, but even within one lesion (44). By recognizing the existence and extent of heterogeneity, PET imaging of a tumor-specific target adds valuable information for individualized treatment decisions.

MSLN-specific tracers have been developed (from different antibodies) for SPECT, as well as PET. A Copper-64 (^{64}Cu)-anti MSLN Fab fragment visualized MSLN-expressing xenografted tumors, as did several Indium-111(^{111}In)-labeled anti-MSLN antibodies (45–48). Moreover, an antibody targeting MSLN was recently conjugated to quantum dots encapsulated in micelles to detect human tumor xenografts in mice (49).

In the preclinical study preceding this clinical trial, ^{89}Zr-MMOT0530A was used for PET imaging of MSLN-expressing human pancreatic tumor xenografts (31). Antigen-specific tracer

Table 1. Patient characteristics at baseline

Characteristics	All patients, n = 11
Pancreatic cancer (n)	7
Ovarian cancer (n)	4
Gender, male/female (n)	2/9
Age (median in years, range)	62, 44–70
Primary tumor *in situ*	
Pancreatic cancer (n)	3
Ovarian cancer (n)	2
Tumor lesions on PET scan	
n, range per patient	37, 1–8
IHC MSLN expression on primary tumor	
n (disease type)	
0	1 (pancreatic cancer)
1+	0
2+	4 (2 ovarian cancer, 2 pancreatic cancer)
3+	2 (1 ovarian cancer, 1 pancreatic cancer)
Unknown	4 (1 ovarian cancer, 3 pancreatic cancer)
IHC MSLN expression on metastatic tumor	
n (disease type)	
0	1 (pancreatic cancer)
1+	0
2+	6 (1 ovarian cancer, 5 pancreatic cancer)
3+	0
Unknown	4 (3 ovarian cancer, 1 pancreatic cancer)

Published OnlineFirst November 20, 2015; DOI: 10.1158/1078-0432.CCR-15-1272

Table 2. ^{89}Zr pharmacokinetics in whole blood samples

Parameter	Mean (±SD) Cohort 1 ($n = 2$)	Mean (±SD) Cohort 2 ($n = 6$)
Cl (L/h)	0.066 (0.014)	0.033 (0.004)
V_d (L)	6.66 (1.433)	4.90 (0.876)
$t_{1/2}$ (h)	70.36 (0.297)	105.17 (22.131)

NOTE: Cohort 1, ∼1 mg ^{89}Zr-labeled MMOT0530A; Cohort 2, ∼1 mg ^{89}Zr-labeled MMOT0530A supplemented with unlabeled MMOT0530A to a total of 10 mg MMOT0530A.

uptake occurred with increasing uptake over time; mean TBR increased from 0.5 via 1.3 to 2.4 at 24, 72, and 144 hours postinjection, respectively.

In general, radionuclide-labeled antibody uptake is higher in tumor lesions of patients than in xenografted animal models. However, in the current clinical study, TBRs in primary pancreatic cancer lesions were relatively low and lower than in the subcutaneously implanted human pancreatic tumors in the preclinical study. This difference may be explained by the higher injected dose of about 1 MBq with 0.5 mg/kg MMOT0530A per mice than the dose administered in humans. In pancreatic cancer, there is a known discrepancy between results in preclinical assays and clinical findings of new drugs. A possible cause might be the influence of the microenvironment in human pancreatic cancer. It has been suggested that the pancreatic stromal tissue diminishes tumor perfusion and thereby tumor penetration and delivery of therapeutics in adequate doses (50). In the preceding preclinical assessment of this tracer, the pancreatic tumors in mice did not contain the same relative amount of stromal tissue as human pancreatic tissue, which may explain the difference in TBR between the preclinical and the current clinical study. Interestingly, primary tumor lesions in pancreatic cancer patients could be visualized, indicating that the antibody did reach these lesions. This was also the case in a recent small

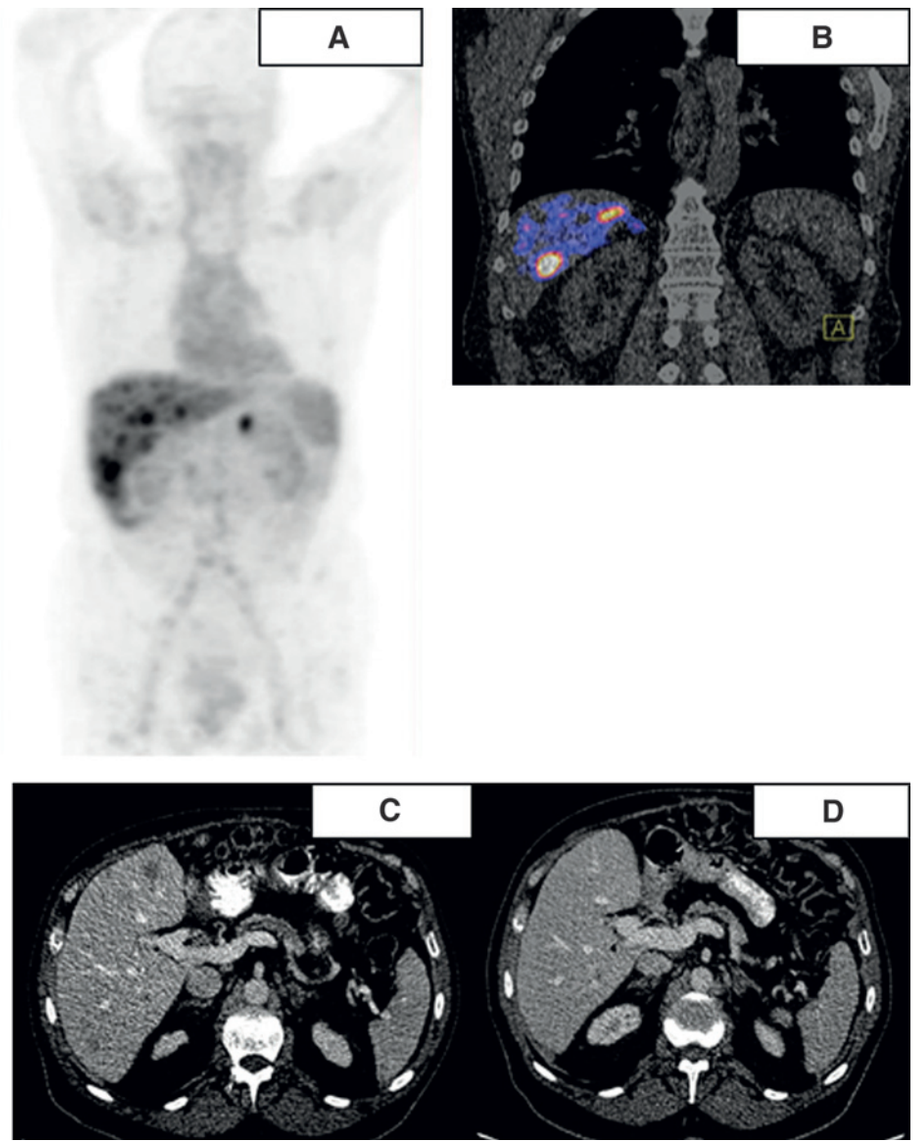

Figure 7.
Images from the patient with pancreatic cancer with liver metastases who has an ongoing partial response according to RECIST 1.1 during the writing of this article. A, maximum intensity projection (MIP) image; B, overlay with CT of the ^{89}Zr-MMOT0530A PET scan performed 4 days postinjection; C, baseline CT scan with liver metastases; D, CT scan after 8 cycles of DMOT4039A treatment, without measurable or visible liver metastases.

study, in 4 patients with mesothelioma and 2 patients with pancreatic cancer. Here, 4 mCi ^{111}In-labeled MSLN antibody amatuximab was administered and subsequent SPECT showed uptake in pancreatic cancer lesions but a higher uptake in mesothelioma lesions (51).

Although not statistically significant, we saw in our study a similar pattern as ^{89}Zr-MMOT0530A PET showed a higher uptake in ovarian cancer lesions compared with pancreatic cancer lesions (mean SUV_{max} of ovarian versus pancreatic lesions were 14.5 versus 11.5, respectively). This might indicate that pancreatic tumor tissue is more difficult to be reached by antibodies than mesothelioma or ovarian cancer lesions, possibly due to extensive stromal tissue in pancreatic cancer.

Moreover, in two patients with pancreatic cancer, the metastatic lesions showed higher tracer uptake than the primary lesions (1.9 and 2.9 fold, respectively). For one of these two patients, both primary and metastatic tissues (a biopsy from lymph nodes) were available for MSLN expression analysis: the primary tumor showed a higher expression (3+) than the metastatic tissue (2+). This again suggests heterogeneity between primary and metastatic lesions, which might explain the differential antibody PET uptake. Overall, immunohistochemical score correlated well to the mean PET uptake in all lesions in a patient.

MSLN expression determined by IHC did not correlate with PET uptake in this study. IHC was performed on archival tumor tissue obtained during surgery or from biopsies. MSLN expression may have changed over time, and intrapatient heterogeneity will likely play a role as well. For a better understanding about the relation between target expression based on IHC and target expression based on PET uptake, fresh tumor biopsies would be most informative. However, this will still provide information about a small part of a tumor lesion, whereas with PET, the whole lesion is being assessed. In addition, other factors such as differences in perfusion can also affect antibody uptake by tumor lesions.

Recently, two ADCs in development for prostate cancer, STEAP1 and TEN2B, have been radiolabeled with ^{89}Zr for PET imaging in mice (52). Tumor tracer uptake was rising in parallel to the efficacy of the ADC treatment, suggesting resembling mechanisms for uptake. As the stability of the ADC is uncertain when both the cytotoxin and the radionuclide are attached to the antibody, we chose to label the naked antibody for PET imaging.

Apart from providing information for early drug development on tracer–antibody organ distribution (and potential organs at risk of toxicity) and tracer–antibody accumulation in the different tumor lesions, this imaging approach might also be of interest in later stages of drug development to select patients that are most likely to benefit from the treatment. As an example, the ZEPHIR study (ClinicalTrials.gov identifier NCT01565200) assesses the predictive value of pretreatment ^{89}Zr-trastuzumab PET in metastatic breast cancer patients before treatment with the ADC T-DM1. In an exploratory patient-based analysis, the combination of ^{89}Zr-trastuzumab PET and an early 18-Fluorine (^{18}F) fluorodeoxyglucose (FDG) PET showed a negative predictive value for RECIST response of 100%, indicating the combined techniques to be promising in identifying patients unlikely to respond to T-DM1. Interestingly, this imaging study also showed highly heterogeneous ^{89}Zr-trastuzumab uptake between and within patients (53).

Given our findings, ^{89}Zr-MMOT0530A PET may be of interest to be used in future trials with DMOT4039A as a complementary tool to select patients with the highest chance of benefit from treatment with DMOT4039A.

Disclosure of Potential Conflicts of Interest

B.M. Fine and D. Maslyar have ownership interest (including patents) in Roche. No potential conflicts of interest were disclosed by the other authors.

Authors' Contributions

Conception and design: L.E. Lamberts, S.P. Williams, B.M. Fine, D. Maslyar, E.G.E. de Vries

Development of methodology: L.E. Lamberts, S.P. Williams, J.R. de Jong, C.P. Schröder, M.N. Lub-de Hooge, E.G.E. de Vries

Acquisition of data (provided animals, acquired and managed patients, provided facilities, etc.): L.E. Lamberts, C.W. Menke-van der Houven van Oordt, F. Bensch, M.M. Smeenk, J. Voortman, O.S. Hoekstra, D. Maslyar, C.P. Schröder, A.H.H. Bongaerts, M.N. Lub-de Hooge, A.W.J.M. Glaudemans, E.G.E. de Vries

Analysis and interpretation of data (e.g., statistical analysis, biostatistics, computational analysis): L.E. Lamberts, C.W. Menke-van der Houven van Oordt, E.J. ter Weele, F. Bensch, M.M. Smeenk, J. Voortman, B.M. Fine, D. Maslyar, J.R. de Jong, J.A. Gietema, C.P. Schröder, S.M. Sanabria Bohorquez, A.W.J.M. Glaudemans, E.G.E. de Vries

Writing, review, and/or revision of the manuscript: L.E. Lamberts, C.W. Menke-van der Houven van Oordt, E.J. ter Weele, F. Bensch, M.M. Smeenk, J. Voortman, O.S. Hoekstra, S.P. Williams, B.M. Fine, D. Maslyar, J.R. de Jong, J.A. Gietema, C.P. Schröder, M.N. Lub-de Hooge, H.M.W. Verheul, S.M. Sanabria Bohorquez, A.W.J.M. Glaudemans, E.G.E. de Vries

Administrative, technical, or material support (i.e., reporting or organizing data, constructing databases): L.E. Lamberts, F. Bensch, M.M. Smeenk, D. Maslyar, C.P. Schröder, A.W.J.M. Glaudemans, E.G.E. de Vries

Study supervision: C.W. Menke-van der Houven van Oordt, H.M.W. Verheul

Acknowledgments

The authors thank Linda Pot, Rianne Bakker, and Annelies Jorritsma for the labeling procedures and Paul van Snick, Cemile Karga, and Marc Huisman for their assistance with PET data transfer.

Grant Support

E.G.E. de Vries received an ERC advanced grant OnQview. Financial support for the study was provided by Genentech to the UMCG.

The costs of publication of this article were defrayed in part by the payment of page charges. This article must therefore be hereby marked *advertisement* in accordance with 18 U.S.C. Section 1734 solely to indicate this fact.

Received May 29, 2015; revised October 16, 2015; accepted October 20, 2015; published OnlineFirst November 20, 2015.

References

1. Hanahan D, Weinberg RA. Hallmarks of cancer: the next generation. Cell 2011;144:646–74.
2. Teicher BA, Chari RV. Antibody conjugate therapeutics: challenges and potential. Clin Cancer Res 2011;17:6389–97.
3. Hassan R, Bera T, Pastan I. Mesothelin: a new target for immunotherapy. Clin Cancer Res 2004;10:3937–42.
4. Chang K, Pastan I. Molecular cloning of mesothelin, a differentiation antigen present on mesothelium, mesotheliomas, and ovarian cancers. Proc Natl Acad Sci U S A 1996;93:136–40.
5. Argani P, Iacobuzio-Donahue C, Ryu B, Rosty C, Goggins M, Wilentz RE, et al. Mesothelin is overexpressed in the vast majority of ductal adenocarcinomas of the pancreas: identification of a new pancreatic cancer

marker by serial analysis of gene expression (SAGE). Clin Cancer Res 2001; 7:3862–8.
6. Ordonez NG. Application of mesothelin immunostaining in tumor diagnosis. Am J Surg Pathol 2003;27:1418–28.
7. Hassan R, Laszik ZG, Lerner M, Raffeld M, Postier R, Brackett D. Mesothelin is overexpressed in pancreaticobiliary adenocarcinomas but not in normal pancreas and chronic pancreatitis. Am J Clin Pathol 2005;124:838–45.
8. Frierson HF Jr, Moskaluk CA, Powell SM, Zhang H, Cerilli LA, Stoler MH, et al. Large-scale molecular and tissue microarray analysis of mesothelin expression in common human carcinomas. Hum Pathol 2003;34:605–9.
9. Kachala SS, Bograd AJ, Villena-Vargas J, Suzuki K, Servais EL, Kadota K, et al. Mesothelin overexpression is a marker of tumor aggressiveness and is associated with reduced recurrence-free and overall survival in early-stage lung adenocarcinoma. Clin Cancer Res 2014;20:1020–8.
10. Tchou J, Wang LC, Selven B, Zhang H, Conejo-Garcia J, Borghaei H, et al. Mesothelin, a novel immunotherapy target for triple negative breast cancer. Breast Cancer Res Treat 2012;133:799–804.
11. Hassan R, Cohen SJ, Phillips M, Pastan I, Sharon E, Kelly RJ, et al. Phase I clinical trial of the chimeric anti-mesothelin monoclonal antibody MORAb-009 in patients with mesothelin-expressing cancers. Clin Cancer Res 2010;16:6132–8.
12. Beatty GL, Haas AR, Maus MV, Torigian DA, Soulen MC, Plesa G, et al. Mesothelin-specific chimeric antigen receptor mRNA-engineered T cells induce antitumor activity in solid malignancies. Cancer Immunol Res 2014;2:112.
13. Hassan R, Bullock S, Premkumar A, Kreitman RJ, Kindler H, Willingham MC, et al. Phase I study of SS1P, a recombinant anti-mesothelin immunotoxin given as a bolus I.V. infusion to patients with mesothelin-expressing mesothelioma, ovarian, and pancreatic cancers. Clin Cancer Res 2007;13:5144–9.
14. Kreitman RJ, Hassan R, Fitzgerald DJ, Pastan I. Phase I trial of continuous infusion anti-mesothelin recombinant immunotoxin SS1P. Clin Cancer Res 2009;15:5274–9.
15. Hassan R, Miller AC, Sharon E, Thomas A, Reynolds JC, Ling A, et al. Major cancer regressions in mesothelioma after treatment with an anti-mesothelin immunotoxin and immune suppression. Sci Transl Med 2013;5: 208ra147.
16. Hassan R, Sharon E, Thomas A, Zhang J, Ling A, Miettinen M, et al. Phase 1 study of the antimesothelin immunotoxin SS1P in combination with pemetrexed and cisplatin for front-line therapy of pleural mesothelioma and correlation of tumor response with serum mesothelin, megakaryocyte potentiating factor, and cancer antigen 125. Cancer 2014;120:3311–9.
17. Bendell J, Blumenschein G, Zinner R, Hong D, Jones S, Infante J, et al. First-in-human phase I dose escalation study of a novel anti-mesothelin antibody drug conjugate (ADC), BAY 94-9343, in patients with advanced solid tumors [abstract]. In: Proceedings of the 104th Annual Meeting of the American Association for Cancer Research; 2013 Apr 6–10; Washington, DC. Philadelphia (PA): AACR; 2013. Abstract nr LB-291.
18. Verma S, Miles D, Gianni L, Krop IE, Welslau M, Baselga J, et al. Trastuzumab emtansine for HER2-positive advanced breast cancer. N Engl J Med 2012;19:1783–91.
19. Tan DS, Thomas GV, Garrett MD, Banerji U, de Bono JS, Kaye SB, et al. Biomarker-driven early clinical trials in oncology: a paradigm shift in drug development. Cancer J 2009;15:406–20.
20. de Vries EG, Oude Munnink TH, van Vugt MA, Nagengast WB. Toward molecular imaging-driven drug development in oncology. Cancer Discov 2011;1:25–8.
21. Lamberts LE, Williams SP, Terwisscha van Scheltinga AG, Lub-de Hooge MN, Schroder CP, Gietema JA, et al. Antibody positron emission tomography imaging in anticancer drug development. J Clin Oncol 2015;33: 1491–504.
22. Wu AM, Olafsen T. Antibodies for molecular imaging of cancer. Cancer J 2008;14:191–7.
23. van Dongen GA, Poot AJ, Vugts DJ. PET imaging with radiolabeled antibodies and tyrosine kinase inhibitors: Immuno-PET and TKI-PET. Tumour Biol 2012;33:607–15.
24. Borjesson PK, Jauw YW, Boellaard R, de Bree R, Comans EF, Roos JC, et al. Performance of immuno-positron emission tomography with zirconium-89-labeled chimeric monoclonal antibody U36 in the detection of lymph node metastases in head and neck cancer patients. Clin Cancer Res 2006; 12:2133–40.
25. Gaykema SB, Brouwers AH, Lub-de Hooge MN, Pleijhuis RG, Timmer-Bosscha H, Pot L, et al. ^{89}Zr-bevacizumab PET imaging in primary breast cancer. J Nucl Med 2013;54:1014–8.
26. Dijkers EC, Oude Munnink TH, Kosterink JG, Brouwers AH, Jager PL, de Jong JR, et al. Biodistribution of ^{89}Zr-trastuzumab and PET imaging of HER2-positive lesions in patients with metastatic breast cancer. Clin Pharmacol Ther 2010;87:586–92.
27. Oosting SF, Brouwers AH, van Es SC, Nagengast WB, Oude Munnink TH, Lub-de Hooge MN, et al. ^{89}Zr-bevacizumab PET visualizes heterogeneous tracer accumulation in tumor lesions of renal cell carcinoma patients and differential effects of antiangiogenic treatment. J Nucl Med 2015;56:63–9.
28. Rizvi SN, Visser OJ, Vosjan MJ, van Lingen A, Hoekstra OS, Zijlstra JM, et al. Biodistribution, radiation dosimetry and scouting of ^{90}Y-ibritumomab tiuxetan therapy in patients with relapsed B-cell non-hodgkin's lymphoma using ^{89}Zr-ibritumomab tiuxetan and PET. Eur J Nucl Med Mol Imaging 2012;39:512–20.
29. Wu AM, Senter PD. Arming antibodies: prospects and challenges for immunoconjugates. Nat Biotechnol 2005;23:1137–46.
30. Ducry L, Stump B. Antibody-drug conjugates: linking cytotoxic payloads to monoclonal antibodies. Bioconjug Chem 2010;21:5–13.
31. Ter Weele EJ, Lub-de Hooge MN, Maslyar D, Terwisscha van Scheltinga AGT, Kosterink JG, de Vries EGE, et al. Imaging human pancreatic tumor xenografts with ^{89}Zr-labeled anti-mesothelin antibody [abstract]. In: Proceedings of the 104th Annual Meeting of the American Association for Cancer Research; 2013 Apr 6–10; Washington, DC. Philadelphia (PA): AACR; 2013. Abstract nr 2659.
32. Borjesson PK, Jauw YW, de Bree R, Roos JC, Castelijns JA, Leemans CR, et al. Radiation dosimetry of ^{89}Zr-labeled chimeric monoclonal antibody U36 as used for immuno-PET in head and neck cancer patients. J Nucl Med 2009;50:1828–36.
33. Makris NE, Boellaard R, van Lingen A, Lammertsma AA, van Dongern GA, Verheul HM, et al. PET/CT derives whole body and bone marrow dosimetry of ^{89}Zr-cetuximab. J Nucl Med 2015;56:249–54.
34. Verel I, Visser GW, Boellaard R, Stigter-van Walsum M, Snow GB, van Dongen GA. ^{89}Zr immuno-PET: comprehensive procedures for the production of ^{89}Zr-labeled monoclonal antibodies. J Nucl Med 2003;44: 1271–81.
35. Eisenhauer EA, Therasse P, Bogaerts J, Schwartz LH, Sargent D, Ford R, et al. New response evaluation criteria in solid tumours: revised RECIST guideline (version 1.1). Eur J Cancer 2009;45:228–47.
36. Weekes C, Lamberts LE, Borad MJ, Voortman J, McWilliams RR, Robinson Diamond J, et al. A phase I study of DMOT4039A, an antibody-drug conjugate (ADC) targeting mesothelin (MSLN), in patients (pts) with unresectable pancreatic (PC) or platinum resistant ovarian cancer (OC). J Clin Oncol 32:5s, 2014 (suppl; abstr 2529).
37. Scales SJ, Gupta N, Pacheco G, Firestein R, French DM, Koeppen H, et al. An antimesothelin-monomethyl auristatin e conjugate with potent antitumor activity in ovarian, pancreatic, and mesothelioma models. Mol Cancer Ther 2014;13:2630–40.
38. Loening AM, Gambhir SS. AMIDE: a free software tool for multimodality medical image analysis. Mol Imaging 2003;2:131–7.
39. Oude Munnink TH, Dijkers EC, Netters SJ, Lub-de Hooge MN, Brouwers AH, Haasjes JG, et al. Trastuzumab pharmacokinetics influenced by extent human epidermal growth factor receptor 2-positive tumor load. J Clin Oncol 2010;28:355–7.
40. Bruno R, Washington CB, Lu JF, Lieberman G, Banken L, Klein P. Population pharmacokinetics of trastuzumab in patients with HER2+ metastatic breast cancer. Cancer Chemother Pharmacol 2005;56:361–9.
41. Zhang Y, Pastan I. High shed antigen levels within tumors: an additional barrier to immunoconjugate therapy. Clin Cancer Res 2008;14:7981–6.
42. Zhang Y, Xiang L, Hassan R, Pastan I. Immunotoxin and taxol synergy results from a decrease in shed mesothelin levels in the extracellular space of tumors. Proc Natl Acad Sci U S A 2007;104:17099–104.
43. Pandit-Taskar N, O'Donoghue JA, Beylergil V, Lyashchenko S, Ruan S, Solomon SB, et al. ^{89}Zr-huJ591 immuno-PET imaging in patients with advanced metastatic prostate cancer. Eur J Nucl Med Mol Imaging 2014;41: 2093–105.
44. Gerlinger M, Rowan AJ, Horswell S, Larkin J, Endesfelder D, Gronroos E, et al. Intratumor heterogeneity and branched evolution revealed by multiregion sequencing. N Engl J Med 2012;366:883–92.

Published OnlineFirst November 20, 2015; DOI: 10.1158/1078-0432.CCR-15-1272

45. Hassan R, Wu C, Brechbiel MW, Margulies I, Kreitman RJ, Pastan I. ^{111}Indium-labeled monoclonal antibody K1: biodistribution study in nude mice bearing a human carcinoma xenograft expressing mesothelin. Int J Cancer 1999;80:559–63.
46. Shin IS, Lee SM, Kim HS, Yao Z, Regino C, Sato N, et al. Effect of chelator conjugation level and injection dose on tumor and organ uptake of ^{111}In-labeled MORAb-009, an anti-mesothelin antibody. Nucl Med Biol 2011;38:1119–27.
47. Misri R, Saatchi K, Ng SS, Kumar U, Hafeli UO. Evaluation of ^{111}In labeled antibodies for SPECT imaging of mesothelin expressing tumors. Nucl Med Biol 2011;38:885–96.
48. Yoshida C, Sogawa C, Tsuji AB, Sudo H, Sugyo A, Uehara T, et al. Development of positron emission tomography imaging by ^{64}Cu-labeled fab for detecting ERC/mesothelin in a mesothelioma mouse model. Nucl Med Commun 2010;31:380–8.
49. Ding H, Yong KT, Law WC, Roy I, Hu R, Wu F, et al. Non-invasive tumor detection in small animals using novel functional pluronic nanomicelles conjugated with anti-mesothelin antibody. Nanoscale 2011;3:1813–22.
50. Feig C, Gopinathan A, Neesse A, Chan DS, Cook N, Tuveson DA. The pancreas cancer microenvironment. Clin Cancer Res 2012;18:4266–76.
51. Lindenberg L, Thomas A, Adler S, Mena E, Kurdziel K, Maltzman J, et al. Safety and biodistribution of ^{111}In-amatuximab in patients with mesothelin expressing cancers using single photon emission computed tomography-computed tomography (SPECT-CT) imaging. Oncotarget 2015;6:4496–504.
52. Ogasawara A, Flores F, Vanderbilt A, Tinianow JN, Gill H, Kan D, et al. Tumor uptake and efficacy of antibody drug conjugates using 89Zirconium ImmunoPET. World Molecular Imaging Congress; 2011 Sept 7–10; San Diego, California: Abstract nr. P822.
53. Gebhart G, Lamberts LE, Garcia C, Ameye L, Stroobants S, Huizing M, et al. PET/CT with ^{89}Zr-trastuzumab and ^{18}F-FDG to individualize treatment with trastuzumab emtansine (T-DM1) in metastatic HER2 positive breast cancer (mBC). J Clin Oncol 32:5s, 2014 (suppl; abstr 11001).

AACR American Association for Cancer Research

Clinical Cancer Research

ImmunoPET with Anti-Mesothelin Antibody in Patients with Pancreatic and Ovarian Cancer before Anti-Mesothelin Antibody–Drug Conjugate Treatment

Laetitia E. Lamberts, Catharina W. Menke-van der Houven van Oordt, Eva J. ter Weele, et al.

Clin Cancer Res 2016;22:1642-1652. Published OnlineFirst November 20, 2015.